Nanoscale Advances

ROYAL SOCIETY OF CHEMISTRY

COMMUNICATION

View Article Online
View Journal | View Issue

Cite this: *Nanoscale Adv.*, 2020, **2**, 2713

Received 8th February 2020
Accepted 18th May 2020

DOI: 10.1039/d0na00107d

rsc.li/nanoscale-advances

Bio-electrostatic sensitive droplet lasers for molecular detection†

Ziyihui Wang,‡[a] Yifan Zhang,‡[b] Xuerui Gong,[b] Zhiyi Yuan,[b] Shilun Feng,[b] Tianhua Xu,[a] Tiegen Liu[a] and Yu-Cheng Chen *[bc]

Electrostatics plays a critical function in most biomolecules, therefore monitoring molecular electrostatic interactions at the biointerface can provide the basis in diagnosis and biomedical science. Herein we report a bioelectrostatic responsive microlaser based on liquid crystal (LC) droplets and explored its application for the ultrasensitive detection of negatively charged biomolecules. A whispering gallery mode (WGM) laser from positively charged LC microdroplets was designed as the optical resonator, in which the lasing wavelength shift was employed as the sensing parameter. We verified that molecular electrostatic changes at the biointerface of the droplet trigger a wavelength shift in laser spectra. Compared to a conventional polarized optical microscope, a significantly improved sensitivity and dynamic range by four orders of magnitude were achieved. Our results helped discover that the surface-to-volume ratio plays a critical role in the detection sensitivity in WGM laser-based microsensors. Finally, bovine serum albumin and specific biosensing were exploited to demonstrate the potential applications of microlasers with a detection limit in the order of 1 pM, thus offering new alternatives for ultrasensitive label-free biosensing and monitoring of molecular interactions.

1. Introduction

Molecular interactions at a biointerface provide the basis for monitoring subtle biomolecular bindings and dynamics. Such interactions include contributions from forces in covalent bonds, non-bonded van der Waals, and electrostatic forces. Among various components of molecular interactions, electrostatics plays a critical function because of its influence on polar or charged molecules, including water, aqueous ions, proteins, nucleic acids, and membrane lipids. Therefore, developing a sensitive method that can respond to the electrostatic changes of biomolecules is of great importance.

Liquid crystals (LCs) are an emerging class of functional materials with a wide variety of biosensing and optoelectrical applications. Thanks to the interactions between liquid crystal and biomolecules, liquid crystals are highly responsive to local molecular anchoring and electrostatics at the interface. Over the past decade, liquid crystals have been extensively applied as a sensing tool to detect proteins,[1–8] nucleic acids,[9–13] acetylcholine,[14,15] glucose,[16–18] and enzymes.[19] Different platforms of liquid crystal biosensors were also developed, such as LC microdroplets[8,16,20–25,29,30] and thin films.[1–7,9–15,17–19,26] The transition of liquid crystal molecules from radial to bipolar orientation can be observed under a polarized optical microscope (POM) upon reaction with molecules.[8,21,24] However, it is often challenging to identify the observable changes of liquid crystal patterns under POM, thus restricting its applications and sensitivity. Recent advances have demonstrated a more sensitive method for detecting the presence of targeted molecules by means of a laser emission spectrum.[22,23,27] Taking advantage of the whispering-gallery-mode (WGM) laser, laser emission-based detection offers unique advantages for strong intensity, narrow linewidth, and high sensitivity to monitor the subtle changes of internal configuration. The LC droplet doped with a dye can support the WGM laser itself and act as a sensing probe. Nevertheless, the detection sensitivity is still minimal, which is comparable to that of conventional POM methods.

In this study, we proposed a novel concept to sensitively detect negatively charged biomolecules by employing positively coated LC droplet microlasers. We systematically demonstrate that the LC-based droplet laser is extremely sensitive to molecular electrostatic interactions. Hence a small change of surface charge will be significantly amplified and cause a lasing wavelength shift. With the dual effect between the whispering-

[a]*School of Precision Instrument and Opto-Electronics, Tianjin University, Tianjin, 300072, China*

[b]*School of Electrical and Electronics Engineering, Nanyang Technological University, 639798, Singapore. E-mail: yucchen@ntu.edu.sg*

[c]*School of Chemical and Biomedical Engineering, Nanyang Technological University, 639798, Singapore*

† Electronic supplementary information (ESI) available. See DOI: 10.1039/d0na00107d

‡ Equal contribution.

gallery mode and liquid crystal, molecular binding signals will be amplified in such LC droplet sensors. The lasing wavelength shift increased as the concentration of molecules increased. We revealed that the surface-to-volume ratio (S/V) plays a major role in governing the sensitivity of a WGM lasing microsensor. The higher the S/V value, the more sensitive the droplet laser can perform to detect molecular electrostatic interactions. Our results clearly proved that the laser spectrum could identify very lower concentrations of label-free molecules, whereas a POM cannot. In comparison to that of state-of-the-art lasers, our sensitivity and dynamic range was significantly improved by over four orders of magnitude. Lastly, we used BSA as an example to demonstrate the sensing capability, in which 0.36 pM (2.4×10^{-11} g ml^{-1}) of BSA molecules were able to be detected due to electrostatic interaction. In addition, specific biosensing was also demonstrated by using streptavidin and biotin. We envision this approach may open new possibilities for the detection of charged biomolecules by providing a lower detection limit than that of conventional methods.

2. Experimental section

2.1 Materials and chemicals

The dye, Coumarin 6 (C6), we used in this study was purchased from Sigma Aldrich (#442631). 4-Cyano-4′-pentylbiphenyl from Tokyo Chemical Industry (#C1550) was used as a nematic liquid crystal (5CB) and sodium dodecyl sulfate (SDS) (Sigma-Aldrich #L3771) as a surfactant. The refractive index of 5CB is 1.53. For the 5CB microdroplet surface modification, poly(4-styrenesulfonic acid) solution (PSS M_w, 75 000 g mol^{-1}) (#561223), poly-L-lysine solution (PLL) (#P4707) and NaOH (#221465) were purchased from Sigma Aldrich. (3-Aminopropyl) triethoxysilane (APTES) (Tokyo Chemical Industry #A0439) was used as a silane coupling agent. *N*-Hydroxysuccinimide (NHS) (Sigma-Aldrich #130672) and *N*-(3-dimethylaminopropyl)-*N*-ethylcarbodiimide hydrochloride (EDC) (Sigma-Aldrich #03450) were used for fixing the droplets on glass slides.

2.2 Preparation of liquid crystal microdroplets

To prepare the dye-doped liquid crystal (LC), 1 mg of coumarin 6 was added to 50 μl of 5CB LC and then mixed in a vortex for 3 minutes. For preparing the LC microdroplet aqueous solution, 50 mg of SDS was added to 50 ml of PBS solution and stirred magnetically for about 20 minutes at 1000 rpm to obtain a homogeneous PBS/SDS solution. To prepare the LC microdroplet emulsion, 50 μl of dye-doped LC was added to 1.4 ml PBS/SDS solution. The resulting mixture was mixed in a vortex for 3 minutes and added into 1 ml PLL solution (concentration: 0.01%), followed by sonication for 15 minutes. After sonication, LC microdroplets were washed with PBS/SDS solution with centrifugation at 5000 rpm for 5 min, and this was repeated 3 times.[24] For the preparation of glass slides, we first cleaned the glass slides using acetone before applying 2% v/v APTES/acetone for a period of 3 min. Then, we washed the slides with ethanol two times and washed them with water. We added 70 mg of NHS and 70 mg of EDC into 26 ml of PBS/SDS solution and put glass slides into the solution; we then added the solution to a Petri dish and placed the glass slides into the solution. To immobilize the microdroplets, 5CB microdroplets were added into the above solution and stored at room temperature for 12 hours.[21] The preparation is also shown in the ESI Fig. S1.†

2.3 Optical setup

Optical pumping was achieved by a pulsed ns-laser (EKSPLA PS8001DR) integrated with an optical parametric oscillator (repetition rate: 50 Hz; pulse duration: 5 ns). Excitation wavelength was 478 nm for all experiments in this work. To pump the 5CB microdroplets and collect light, an inverted microscopic system (Nikon Ti2) with a 20× 0.4 NA objective was used. The collected light was sent to a charge-coupled device camera or an imaging spectrometer (Andor Kymera 328i and Newton 970 EMCCD).

3. Results and discussion

3.1 Spectral response of the LC droplet induced by molecular electrostatic interactions

First, we investigated how the positively charge coated LC microdroplet responds to molecular electrostatic interactions by means of the laser emission spectrum. As such, poly-L-lysine (PLL) was used to form a positively charged surface on the LC droplet throughout the entire study. A schematic diagram of the experimental setup is shown in Fig. 1(a), where the surface of the C6-doped LC droplet carried positive charges due to PLL. With the advent of negative charges from biomolecules, the internal orientation of liquid crystal molecules transforms from radial to bipolar, as shown in Fig. 1(b). As such, it is expected that the WGM laser spectrum will shift with the corresponding electrostatic changes (Fig. 1(c)), and therefore, it could be employed as a sensing signal for biosensing.

To modify the surface charges on the LC droplet, small amounts of PSS solution (anionic polyelectrolyte, 10^{-3} g ml^{-1}) were added to the surrounding solution gradually (Fig. 1(d)). The association of PSS to the PLL coated microdroplet would result in the reduction of positively charged groups on the surface and change the internal configuration of the LC microdroplet. Fig. 1(e) presents the laser spectrum captured from a single droplet before and after the addition of PSS molecules. It was found that the spectrum of the 5CB microdroplet underwent a rapid and significant wavelength shift. Next, we investigated under different concentrations of PSS molecules separately by selecting the same droplet size (13 ± 0.5 μm). The corresponding wavelength shift is plotted against PSS concentrations from 10^{-3} g ml^{-1} to 10^{-8} g ml^{-1}. All of which were measured at $t = 40$ s when the laser peaks become stable, as shown in Fig. 1(f). Our results manifest a strong linear dependence of the spectral shift on PSS concentrations, whereby the spectral response was found to become more obvious as the concentration increased. As a control group, we also conducted the same experiment by using different concentrations of the OH^- solution (Fig. 1(d)). To confirm that the changes in the LC droplet were induced by surface charges,

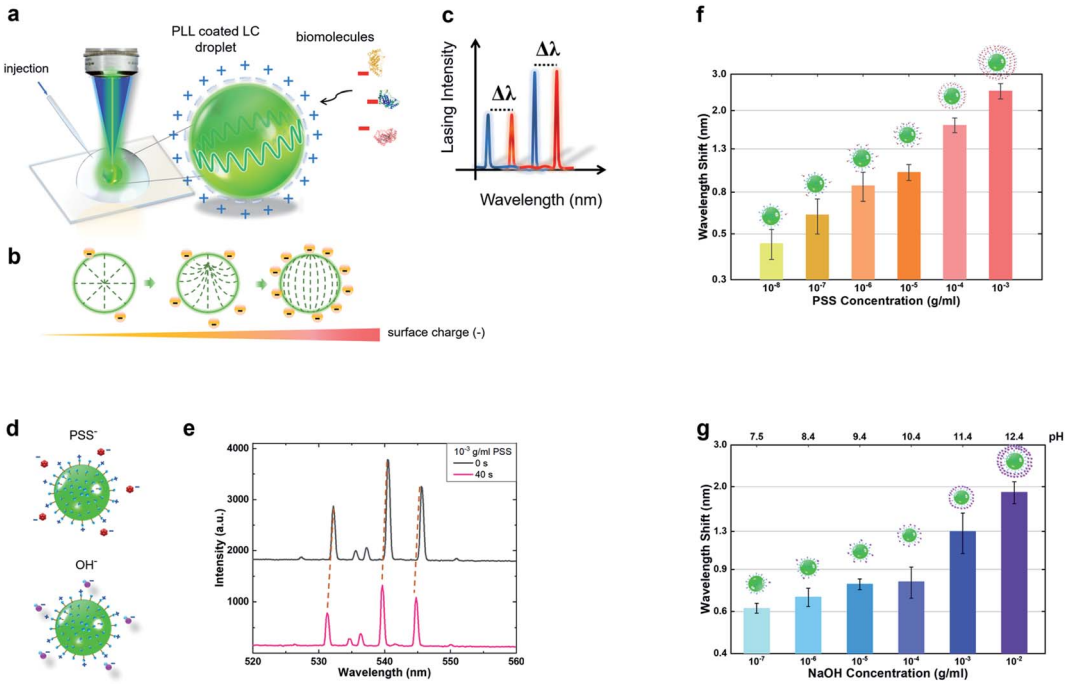

Fig. 1 (a) Schematic diagram of the experimental design and setup. The fixed liquid crystal droplet (doped with C6) was fixed on a glass slide and excited by a pump laser. Excitation wavelength = 478 nm. A pipette tip was used for dripping the quantitative solution. The microdroplet was coated with PLL to form a positively charge surface, which would attract negatively charged molecules. (b) The lines represent the orientation of the long axes of the LC molecules. By increasing the negative surface charges, the surface anchoring of LC molecules gradually changes towards the homeotropic molecular orientation, from radial to bipolar. (c) With the increment of surface charges, the spectrum of the WGM lasing emission is expected to shift ($\Delta\lambda$). (d) PSS molecules and OH^- ions were used as a model to study the surface charge effect (molecular electrostatic) to the LC microdroplet, respectively. (e) Laser spectra of a fixed LC microdroplet before and after adding 10^{-3} g ml^{-1} PSS solution for 40 seconds. (f) Summary of the wavelength shift for the LC droplet with various concentrations of PSS molecules. (g) Summary of the wavelength shift for the LC droplet with various concentrations of NaOH (OH^- ions). The corresponding pH values are provided on the top *x*-axis accordingly. Observation time point = 40 seconds.

similarly, we analysed the relationship between OH^- concentrations from 10^{-2} g ml^{-1} to 10^{-7} g ml^{-1}. When adding NaOH, the pH of the solution changes accordingly (Fig. 1(g)). Munir *et al.*[28] and Wang *et al.*[23] showed that the effect of pH values on the configuration of the liquid crystal droplet is essentially the change of charge density. A consistent trend was also observed for different OH^- concentrations, implying that surface charges play an important factor for wavelength shifting. The changes in laser spectra can be attributed to the adsorption of anions at the LC droplet surface, which perturbs the intermolecular interactions and thus reorients the LC configuration. Consequently, the responses of laser spectra induced directly by LC structural transition intuitively reflect the ambient electronegativity variations.

3.2 Effect of surface-to-volume ratio on detection sensitivity

In order to understand the critical factors in detection sensitivity, we studied the impact of the surface-to-volume (S/V) ratio towards the wavelength shift under electrostatic interaction. Since the S/V ratio depends on the diameter of the LC microdroplet, different diameters of droplets were selected by applying the same concentration of PSS molecules (10^{-5} g ml^{-1}). For demonstration, Fig. 2(a) and (b) present the WGM laser spectrum generated from a 9 μm droplet and 40 μm droplet, respectively. It is obvious that the 9 μm droplet exhibited a larger wavelength shift than the 40 μm droplet due to a higher S/V ratio. Note that the minimum size which can support LC lasing is approximately 7 μm; here we selected the 9 μm droplet for example. Moreover, we compared the lasing wavelength shift based on different S/V ratios from different diameters of LC droplets (9 μm/12 μm/16 μm/20 μm/25 μm/30 μm/40 μm). The relationship between the wavelength shift and S/V ratio is plotted in Fig. 2(c). Our results demonstrate that the S/V ratio has a clear effect on the sensitivity of molecular detection. The larger the S/V ratio, the more internal orientation of liquid crystal molecules will be changed, thus affecting the extent of resonant wavelength. As such, both the sensitivity and detection limit could be significantly improved by increasing the S/V ratio of the microcavity.

3.3 Potential application for protein molecule sensing

Based on the previous section, here, we also explored the potential for biosensors based on the PLL coated 5CB microdroplets. Since most biomolecules contain molecular electrostatic interactions, the proposed platform possesses the potential to detect a large number of negatively charged biomolecules. Here we used BSA as a target molecule for a proof-of-concept. To examine the effects of the PLL coated LC

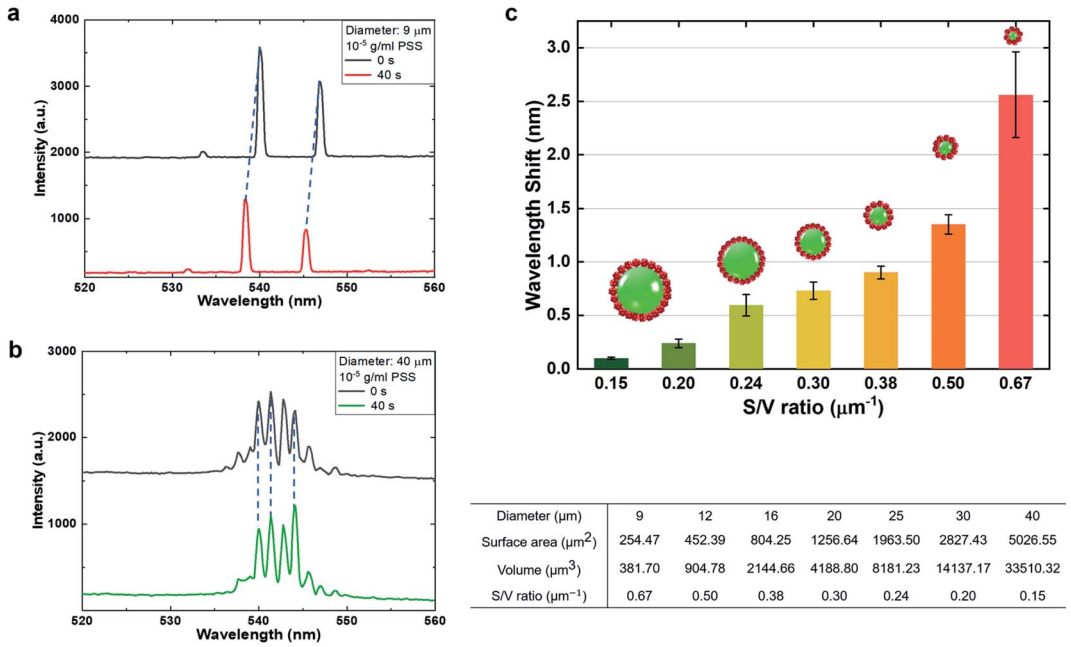

Diameter (μm)	9	12	16	20	25	30	40
Surface area (μm^2)	254.47	452.39	804.25	1256.64	1963.50	2827.43	5026.55
Volume (μm^3)	381.70	904.78	2144.66	4188.80	8181.23	14137.17	33510.32
S/V ratio (μm^{-1})	0.67	0.50	0.38	0.30	0.24	0.20	0.15

Fig. 2 Effect of the surface-to-volume (S/V) ratio on spectral responses. (a and b) Laser spectra before and after applying 10^{-5} g ml^{-1} PSS molecules to a LC droplet of (a) 9 μm diameter and (b) 40 μm diameter, separately. (c) Comparison of the lasing wavelength shift as a function of different S/V ratios. The bottom panel shows the relationship between the 5CB droplets of various diameters and the corresponding S/V ratio.

microdroplet on BSA detection, Fig. 3(a) demonstrates the spectral response of the LC droplet with 10^{-4} g ml^{-1} BSA, where a huge wavelength shift can be seen. The corresponding POM images are shown in the inset. As one can see, the droplet changed from radial to bipolar orientation. Next, we tested a lower concentration of BSA, down to 10^{-10} g ml^{-1} (1.5 pM) in Fig. 3(b). Although much smaller than Fig. 3(a), a wavelength shift was still observed when collected under the same time interval. However, it is noteworthy that the corresponding POM images in the insets do not show observable changes in terms of liquid crystal orientation. It is believed that the slight changes in terms of the LC orientation are too little to cause the entire droplet to form observable patterns. In addition, we also tested 0 mg ml^{-1} BSA as a control experiment (ESI Fig. S2†). Only an extremely small wavelength shift ($\ll$0.1 nm) was detected, manifesting the reliability of the laser-based detection.

Finally, we studied the WGM spectral responses of the LC microdroplet under different BSA concentrations. The spectral responses of typical traces from three different BSA concentrations (10^{-4} g ml^{-1}, 10^{-6} g ml^{-1} and 10^{-10} g ml^{-1}), were recorded over 60 seconds. For each concentration, three traces were tested and exhibited similar tendencies, as shown in Fig. 3(c). As one can see, the total wavelength shift is similar under the same concentration, regardless of the transition interval. At a higher BSA concentration (10^{-4} g ml^{-1}), the laser peaks blue shift within 0.5 nm in the first several seconds, a redshift of 5.3 nm was seen until stabilized. At a relatively lower concentration (10^{-6} g ml^{-1}), a blue shift of 0.55 nm was observed at first, then began to redshift gradually. Under very low BSA concentration (10^{-10} g ml^{-1}), the spectral response only presented a blue-shift tendency with a wavelength shift of 0.23 nm. Among all the data collected, laser peaks were found to become stabilized after 40 s. As such, here we presented a time interval of wavelength shift over 1 minute (60 s), representing the equilibrium of LC microdroplets.

Subsequently, we repeated the above process and measured the spectral response the of wavelength shift under various BSA concentrations (10^{-10} g ml^{-1} to 10^{-4} g ml^{-1}). As both blue and red shifts occur in many cases, it is more reasonable to calculate the total laser peak wavelength shift, (defined as blue shift + red shift). According to the literature, there are no explanations yet as to why sometimes blue and sometimes red shifts occur. However, for the first time, we observed this very interesting phenomenon (shown in Fig. 3(c)). We further discovered that the total wavelength shift increased proportionally with the BSA concentrations. The total wavelength shifts of the laser spectrum against BSA concentrations are plotted in the logarithmic axis, as shown in Fig. 3(d), all of which were based on an average of three traces over 60 s. The total wavelength shift was found to have a linear dependence on BSA concentrations. Based on a fixed droplet size (13 $\pm$ 0.5 μm), the maximum wavelength shift detected was approximately 5.45 nm under 0.1 mg ml^{-1} BSA. In addition, the limit of detection (LOD) was calculated to be 0.36 pM (2.4×10^{-11} g ml^{-1}) by $3\alpha/k$, where α is the standard error ($\alpha = 0.018$) of the blank and k is the slope ($k = 0.22$) of the calibration curve in Fig. 3(d). Here we would like to mention that both red and blue shifts have been reported in the literature; however, the main reason is still unclear. It is believed that the presence of either blue or red shifts is the result of orientation changes in LC molecules. As a comparison, a polarized optical microscope was used to record LC droplets under the same BSA concentrations with fixed conditions. Fig. 3(e) shows the POM images of individual LC microdroplets when immersed in the respective BSA concentrations after 40

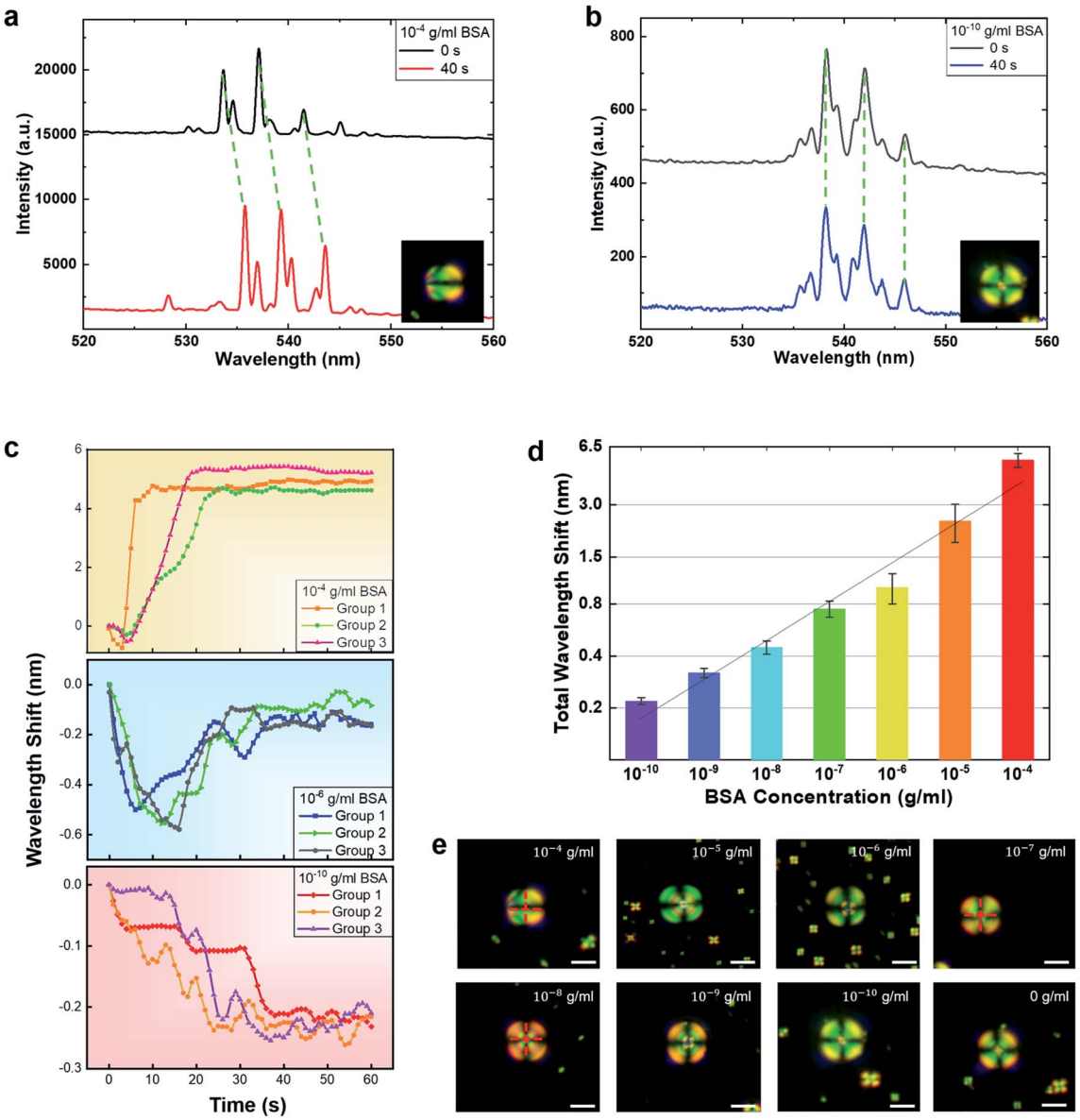

Fig. 3 (a) WGM laser spectra of the LC microdroplet before (black curve) and after adding 10^{-4} g ml^{-1} of BSA (red curve). (b) WGM laser spectra of the LC microdroplet before (black curve) and after adding 10^{-10} g ml^{-1} of BSA (purple curve). (c) Real-time monitoring of the laser spectral shift of the LC droplet under representative BSA concentrations (10^{-10}, 10^{-6}, and 10^{-4} g ml^{-1}) over 60 seconds. Three traces were tested for each concentration. (d) The total wavelength shift (accumulative distance by adding the blue shift and red shift) extracted from laser spectra based on the average of three traces for each BSA concentration. The limit of detection was calculated to be 0.36 pM according to the calibration curve. (e) Polarized optical images of the corresponding LC microdroplet under various concentrations (10^{-4}, 10^{-5}, 10^{-6}, 10^{-7}, 10^{-8}, 10^{-9}, 10^{-10} g ml^{-1}, and 0 g ml^{-1}) of BSA. Scale bars, 10 μm.

seconds. Apparently, the lowest detection limit for observable changes in the POM is about 10^{-7} g ml^{-1}. For concentrations below 10^{-7} g ml^{-1}, we can barely see any significant difference in terms of the polarization changes. For concentrations above 10^{-7} g ml^{-1}, POM can clearly observe the LC transitions between radial to bipolar. As such, the results here demonstrated that the WGM laser spectrum is four orders more sensitive than that of the POM in terms of molecular electrostatic interactions. To demonstrate the capability for biosensing, we presented a set of specific binding experiments by using strepavidin (SA) and biotin. By coating SA on the LC droplet, the spectral shift increases linearly with the binding biotin concentrations (ESI Fig. S3†). Hence, we envisage liquid crystal WGM microlasers having the potential to provide much-improved sensitivity and dynamic range for the detection of a wide range of biomolecules.

4. Conclusion

In this research, we developed a bio-electrostatic responsive liquid crystal droplet microlaser for ultrasensitive detection of biomolecules. The concept proposed here can be widely applied

to a wide range of biomolecules, such as DNA, proteins, and small molecules. We verified that molecular electrostatic interactions at the biointerface of the liquid crystal droplet could trigger a wavelength shift in WGM laser spectra. The total wavelength shift increased proportionally with the adhering PSS/OH^- molecule concentration. Our findings also revealed that the surface-to-volume ratio has a significant impact on the detection sensitivity of WGM laser microsensors. Finally, by employing BSA as an example of a negatively charged biomolecule, the total wavelength shift increased proportionally with the BSA concentrations with a detection limit of 0.36 pM. It is expected that a lower detection limit can be achieved by using a higher-resolution spectrometer (<0.1 nm). In comparison to current reported LC sensors and conventional POM techniques, our sensitivity and dynamic range significantly improved by four orders of magnitude, thus offering a promising tool for label-free molecular biosensing.

Conflicts of interest

The authors declare no competing financial interests.

Acknowledgements

The authors would like to acknowledge the support from Professor Yu-Chieh Cheng at the National Taipei University of Science and Technology for instruction of liquid crystal laser fabrication. We also acknowledge the financial support from the NTU Research Startup grant SUG 4082308.040.

References

1 Y.-L. Chiang, M.-J. Lee and W. Lee, Enhancing detection sensitivity in quantitative protein detection based on dye-doped liquid crystals, *Dyes Pigm.*, 2018, **157**, 117–122.
2 Q. He, H. Lei, S. Luo, P. Tang, X. Peng and X. Wang, Liquid crystal biosensor for detecting ischemia modified albumin, *Res. Chem. Intermed.*, 2016, **43**(1), 353–360.
3 W. Zhang, W. T. Ang, C. Y. Xue and K. L. Yang, Minimizing nonspecific protein adsorption in liquid crystal immunoassays by using surfactants, *ACS Appl. Mater. Interfaces*, 2011, **3**(9), 3496–3500.
4 Y. Wang, Q. Hu, T. Tian, Y. Gao and L. Yu, A nonionic surfactant-decorated liquid crystal sensor for sensitive and selective detection of proteins, *Anal. Chim. Acta*, 2016, **937**, 119–126.
5 C.-H. Lin, M.-J. Lee and W. Lee, Bovine serum albumin detection and quantitation based on capacitance measurements of liquid crystals, *Appl. Phys. Lett.*, 2016, **109**(9), 093703.
6 M.-J. Lee and W. Lee, Liquid crystal-based capacitive, electro-optical and dielectric biosensors for protein quantitation, *Liq. Cryst.*, 2019, 1–9.
7 Y. C. Hsiao, Y. C. Sung, M. J. Lee and W. Lee, Highly sensitive color-indicating and quantitative biosensor based on cholesteric liquid crystal, *Biomed. Opt. Express*, 2015, **6**(12), 5033–5038.
8 I. Verma, S. Sidiq and S. K. Pal, Protein triggered ordering transitions in poly (L-lysine)-coated liquid crystal emulsion droplets, *Liq. Cryst.*, 2019, **46**(9), 1318–1326.
9 S. Yang, Y. Liu, H. Tan, C. Wu, Z. Wu, G. Shen and R. Yu, Gold nanoparticle based signal enhancement liquid crystal biosensors for DNA hybridization assays, *Chem. Commun.*, 2012, **48**(23), 2861–2863.
10 H. Tan, S. Yang, G. Shen, R. Yu and Z. Wu, Signal-enhanced liquid-crystal DNA biosensors based on enzymatic metal deposition, *Angew. Chem.*, 2010, **49**(46), 8608–8611.
11 M. Khan, A. R. Khan, J. H. Shin and S. Y. Park, A liquid-crystal-based DNA biosensor for pathogen detection, *Sci. Rep.*, 2016, **6**, 22676.
12 J. Zhou, Y. Dong, Y. Zhang, D. Liu and Z. Yang, The Assembly of DNA Amphiphiles at Liquid Crystal-Aqueous Interface, *Nanomaterials*, 2016, **6**(12), 229.
13 J. Shen, F. He, L. Chen, L. Ding, H. Liu, Y. Wang and X. Xiong, Liquid crystal-based detection of DNA hybridization using surface-immobilized single-stranded DNA, *Microchim. Acta*, 2017, **184**(9), 3137–3144.
14 G.-R. Han and C.-H. Jang, Liquid crystal sensor for the detection of acetylcholine using acetylcholinesterase immobilized on a nanostructured polymeric surface, *Colloid Polym. Sci.*, 2015, **293**(10), 2771–2779.
15 S. Liao, Y. Qiao, W. Han, Z. Xie, Z. Wu, G. Shen and R. Yu, Acetylcholinesterase liquid crystal biosensor based on modulated growth of gold nanoparticles for amplified detection of acetylcholine and inhibitor, *Anal. Chem.*, 2012, **84**(1), 45–49.
16 J. Kim, M. Khan and S. Y. Park, Glucose sensor using liquid-crystal droplets made by microfluidics, *ACS Appl. Mater. Interfaces*, 2013, **5**(24), 13135–13139.
17 M. Khan and S. Y. Park, Liquid crystal-based glucose biosensor functionalized with mixed PAA and QP4VP brushes, *Biosens. Bioelectron.*, 2015, **68**, 404–412.
18 M. Khan and S. Y. Park, Liquid crystal-based proton sensitive glucose biosensor, *Anal. Chem.*, 2014, **86**(3), 1493–1501.
19 R. Duan, X. Hao, Y. Li and H. Li, Detection of acetylcholinesterase and its inhibitors by liquid crystal biosensor based on whispering gallery mode, *Sens. Actuators, B*, 2020, **308**, 127672.
20 X. Niu, D. Luo, R. Chen, F. Wang, X. Sun and H. Dai, Optical biosensor based on liquid crystal droplets for detection of cholic acid, *Opt. Commun.*, 2016, **381**, 286–291.
21 Y. Huan, S. J. Park, K. Chandra Gupta, S.-Y. Park and I.-K. Kang, Slide cover glass immobilized liquid crystal microdroplets for sensitive detection of an IgG antigen, *RSC Adv.*, 2017, **7**(60), 37675–37688.
22 R. Duan, Y. Li, B. Shi, H. Li and J. Yang, Real-time, quantitative and sensitive detection of urea by whispering gallery mode lasing in liquid crystal microdroplet, *Talanta*, 2020, **209**, 120513.
23 Y. Wang, L. Zhao, A. Xu, L. Wang, L. Zhang, S. Liu, Y. Liu and H. Li, Detecting enzymatic reactions in penicillinase *via* liquid crystal microdroplet-based pH sensor, *Sens. Actuators, B*, 2018, **258**, 1090–1098.

24 S. Sidiq, G. Prasad, A. Mukhopadhaya and S. K. Pal, Poly(l-lysine)-Coated Liquid Crystal Droplets for Cell-Based Sensing Applications, *J. Phys. Chem. B*, 2017, **121**(16), 4247–4256.

25 J. A. Sofi and S. Dhara, Stability of liquid crystal micro-droplets based optical microresonators, *Liq. Cryst.*, 2018, **46**(4), 629–639.

26 M. Tyagi, A. Chandran, T. Joshi, J. Prakash, V. V. Agrawal and A. M. Biradar, Self assembled monolayer based liquid crystal biosensor for free cholesterol detection, *Appl. Phys. Lett.*, 2014, **104**(15), 154104.

27 M. Humar and I. Musevic, Surfactant sensing based on whispering-gallery-mode lasing in liquid-crystal microdroplets, *Opt. Express*, 2011, **19**, 19836–19844.

28 S. Munir and S. Y. Park, Label- and enzyme-free detection of glucose by boronic acid-coupled poly(styrene-b-acrylic acid) at liquid crystal/aqueous interfaces, *Anal. Chim. Acta*, 2018, **1032**, 122–129.

29 Y. C. Chen and X. Fan, Biological Lasers for Biomedical Applications, *Adv. Opt. Mater.*, 2019, **7**(17), 1900377.

30 Z. Yuan, Z. Wang, P. Guan, X. Wu and Y. C. Chen, Lasing-Encoded Microsensor Driven by Interfacial Cavity Resonance Energy Transfer, *Adv. Opt. Mater.*, 2020, 1901596.